Published in final edited form as:
NMR Biomed. 2009 April ; 22(3): 332–341. doi:10.1002/nbm.1343.

Blood-Spinal Cord Barrier Permeability in Experimental Spinal Cord Injury: Dynamic Contrast-Enhanced Magnetic Resonance Imaging

David M. Cohen[†], **Chirag B. Patel**[†], **Pallavi Ahobila-Vajjula**, **Laura M. Sundberg**, **Tessy Chacko**, **Shi-Jie Liu**, and **Ponnada A. Narayana**[1]
Department of Diagnostic and Interventional Imaging University of Texas Medical School at Houston 6431 Fannin Street, Houston, TX 77030

Abstract

Following the primary traumatic injury, spinal cord tissue undergoes a series of pathobiological changes, including compromised blood-spinal cord-barrier (BSCB) integrity. These vascular changes occur over both time and space. In an experimental model of spinal cord injury (SCI), longitudinal dynamic contrast-enhanced magnetic resonance imaging (DCE-MRI)studies were performed up to 56 days post-SCI to quantify spatial and temporal changes in the BSCB permeability in tissue that did not show any visible enhancement on the post-contrast MRI(non-enhancing tissue). DCE-MRI data was analyzed using a two-compartment pharmacokinetic model. These studies demonstrate gradual restoration of BSCB with post-SCI time. But, based on DCE-MRI, and confirmed by immunohistochemistry, the BSCB remained compromised even at 56 days post-SCI. In addition, open-field locomotion was evaluated using the 21 point Basso-Beattie-Bresnahan scale. A significant correlation between decreased BSCB permeability and improved locomotor recovery was observed.

Keywords

spinal cord injury; blood-spinal cord barrier; rodents; dynamic contrast-enhanced MRI; focal enhancement; diffuse enhancement; normal appearing white matter; BBB score

INTRODUCTION

The central nervous system (CNS) responds to traumatic spinal cord injury (SCI) in complex ways (1). The primary mechanical injury results in axonal and vascular damage at the site of contusion and is generally considered to be irreversible. Subsequently, a series of pathobiological events is initiated in response to the primary insult that further damages the issue both at and around the site of injury (2,3).

The secondary injury cascades following mechanical trauma include dynamic vascular changes that are known to occur as both early and delayed events (4-14). These vascular changes contribute to the secondary pathogenesis that influence the chronic functional deficits observed in SCI. Specifically, these vascular events include changes in blood flow, intraparenchymal hemorrhage, inflammation, disruption of the blood-spinal cord barrier (BSCB), and angiogenesis. In these studies we have focused on the role of the BSCB in SCI.

[1]Corresponding Author Telephone: (713) 500-7677 Email: ponnada.a.narayana@uth.tmc.edu.
[†]These authors contributed equally to this work

The BSCB exists at the capillary level and regulates the molecules that can enter the tissue, thereby protecting it from neurotoxins in systemic circulation (15,16). In fact, one of the earliest events following traumatic SCI is the disruption of the BSCB. The compromised barrier is detrimental to tissue recovery. A number of studies have also demonstrated that BSCB disruption lasts up to 28 days following the initial injury and spreads along the length of the cord (11,17,18). The extended time course of BSCB breakdown has also been confirmed by magnetic resonance imaging (MRI) (19,20).

Traditionally, vascular plasticity has been assessed using large cohorts of animals, sacrificing groups of them at multiple time points. While such approaches provide critical information with high spatial resolution about the ongoing microvascular remodeling, they are limited to providing only static “snap shots” of the post-injury environment. Dynamic contrast-enhanced magnetic resonance imaging (DCE-MRI) is a powerful noninvasive technique that enables quantification of BSCB permeability (4,19,20). Because of its noninvasive nature, this technique allows probing of temporal and spatial changes in the BSCB permeability in the same group of animals. DCE-MRI involves repeated acquisition of T1-weighted MR images following the intravenous administration of a paramagnetic contrast agent such as gadopentate dimeglumine (Gd) (21). In intact vasculature, these contrast agents are confined within the systemic circulation and do not cross the BSCB. However, in the presence of compromised BSCB, the contrast agent escapes into the interstitial space that results in regionally increased signal intensity in the T1-weighted images. Using an appropriate pharmacokinetic model (19), the temporal changes in the contrast agent-induced signal increase can be quantitatively related to the BSCB permeability.

Following the administration of Gd, two types of intensity changes are visually observed in the spinal cord tissue on T1-weighted images (4,19): 1) diffuse enhancement (DE) which results from mechanically disrupted vasculature and is mainly confined to and around the site of primary injury and 2) focal enhancements (FE) that are the result of leaky angiogenic vessels and are generally observed two weeks after SCI, mainly confined to the spinal cord white matter (WM) (10). Much of the tissue that is about 3 mm away from the site of injury does not show any enhancement (non-enhancing (NE)), at least visually, suggesting lack of gross disruption of the BSCB. However, the BSCB in the NE tissue may still be compromised. Quantitative analysis of DCE-MRI studies allow for the non-invasive quantification of spatial and temporal changes in BSCB permeability and assessment of microvascular integrity in this non-enhancing tissue. In these studies we have focused on the NE area because its role in the progression of secondary injury in SCI is not known.

The application of DCE-MRI studies for estimation of BSCB permeability in SCI was reported by Bilgen et al. in the acute phase as well as up to 30 days post-injury (4,19). Those studies showed that BSCB permeability was compromised even at day 30 post-SCI and that BSCB permeability was inversely correlated with the neurobehavioral status, as assessed by the modified Tarlov score (22). Those studies mainly concentrated on tissues that exhibited enhancement on post-contrast images and assessed only the global changes. In contrast, the main focus of our studies is the spatial and temporal changes in the BSCB in tissue that does not visually exhibit post-contrast enhancement. We hypothesize that the BSCB of spinal cord regions that are away from the site of injury, but do not exhibit enhancement, is compromised and this compromised BSCB plays an important role in the progression of secondary injury. In order to verify this hypothesis we have quantified the BSCB permeability of the non-enhancing tissue by analyzing DCE-MRI and correlated the BSCB permeability with behavioral outcome as assessed by the Basso-Beattie-Bresnahan (BBB) score (23).

EXPERIMENTAL

The protocol employed in these studies was approved by the institutional Animal Welfare Committee. All animal procedures were performed according to the NIH Guide for the Care and Use of Laboratory Animals.

Spinal Cord Injury

Male Sprague-Dawley rats (300-350 g) were anesthetized with spontaneous inhalation of isoflurane (4%). They were then intubated and maintained under anesthesia by mechanical ventilation with 2% isoflurane, 30% O_2, and 68% air. Under anesthesia, a single spinous process and the corresponding laminae at the T7 level were surgically removed. The spinal cord was exposed and a moderately severe injury at the T7 level was produced using an in-house developed injury device that has been shown to produce consistent injuries (10). Briefly, the injury device was designed to produce contusive-type injury and is based on a linear motor (P01-23×80LinMot Inc., Zurich, Switzerland) mounted on an x-y-z platform (Sherline Products Inc., Vista, CA). The tip of the injury bit measured 0.5 mm × 0.5 mm. The mechanical parameters were impact speed of bit = 1.5 m/sec, cord compression = 1.7 mm, and duration of compression = 80 ms. These mechanical parameters were shown to produce a moderately severe injury to the spinal cord (10).

For improved SNR in MRI, a 11 mm × 27 mm radiofrequency (RF) coil tuned to 300 MHz was implanted subcutaneously over the injury site, without touching the spinal cord (24). The wound was closed in two layers using absorbable sutures. To enable intravenous delivery of contrast agent (Magnevist, Berlex Laboratories, Montville, NJ) during the DCE-MRI scans, the right jugular vein was cannulated and a vascular port with silicone tubing (Instech Solomon, Plymouth Meeting, PA) was implanted. The catheter was secured with a 4-0 silk suture. At the end of the catheter a two way valve was connected for administering Gd and saline chase. The reservoir of the jugular port was implanted subcutaneously in the right chest region and skin incisions were closed with 4-0 Vicryl sutures.

Animal Care

Animals were allowed to recover in warmed cages and received saline subcutaneously (10 mL after anesthesia wore off and 5 mL eight hours later). The manual subcutaneous hydration schedule was 5 mL twice daily for 1-2 days post-SCI, 4 mL twice daily for 3-4 days post-SCI, and 3 mL twice daily for 5 days post-SCI. Thereafter, hydration in the rats was monitored. Animals received Baytril-100 (2.5 mg/kg, Bayer Healthcare LLC Animal Division, Shawnee Mission, KS) subcutaneously twice daily for 0-3 days post-SCI and Buprenex (0.01 mg/kg, Hospira Inc., Lake Forest, IL) subcutaneously twice daily for 5 days post-SCI. While animals had free access to food and water, if they were found to be starving and/or dehydrated, aminoplex and/or fluids were administered subcutaneously. Animals' urinary bladders were manually expressed every 12 hours until the return of spontaneous urination. Zinc oxide ointment (E. Fougera & Co., Melville, NY) was applied if the skin appeared irritated. Triple antibiotic ointment (Alpharma USPD Inc., Baltimore, MD) was applied on wounds or broken skin. When necessary, rats were gently bathed with hypoallergenic shampoo (HydroSurge, Carlsbad, CA) and warm water.

MRI Protocol

All MR studies were performed on a 7 Tesla Bruker scanner (70/30 USR Bruker Biospec, Karlsruhe, Germany) using a 116 mm shielded gradient insert that is capable of producing maximum gradient amplitude of 400 mT/m with 80 μs rise time. On MRI scan days, animals were anesthetized with an induction dose of 4% isoflurane and were then intubated and mechanically ventilated with 2-2.5% isoflurane, 30% oxygen and 67.5-68% air (rodent

ventilator, model 683, Harvard Apparatus, Holliston, MA) for the duration of the scan (approximately 3 hours). Rats were placed in the supine position on a Plexiglas bed and an in-house designed 35 mm × 40 mm linear surface coil (24) was placed under the rat and was inductively coupled to the implanted RF coil. Silicone tubing (Instech Solomon, Plymouth Meeting, PA) was attached to the jugular port while the other end of the tubing was attached to a two-way valve. The two ports of the valves were each connected to a syringe, one of which was filled with Gd (Magnevist, Berlex Laboratories, Montville, NJ) at a concentration of 287 mg/kg and the other of which was filled with 0.9% saline. The tubing was long enough to allow administration of Gd without moving the animal bed during the MRI scan. Following the acquisition of a tri-pilot scan (for locating the spinal cord) and anatomical scans, pre-contrast T1-weighted spin echo, axial images were acquired with the following parameters: repetition time (TR) = 500 ms, echo time (TE) = 10.4 ms, field-of-view (FOV) = 2.6 cm × 2.6 cm, slice thickness = 1 mm, and acquisition matrix = 256×128 (zero-filled to 256×256). Then a 0.2 mL bolus of Gd was injected in less than 5 s into the jugular vein via the vascular port. Immediately following the administration of Gd, T1-weighted images were acquired continuously with identical geometry and scan parameters were acquired at 30 time points with a temporal resolution of 2 minutes, as part of the DCE-MRI scan. The total scan time for a DCE-MRI study was thus approximately 60 minutes.

Prior to performing each DCE-MRI scan, a quality assurance scan that included SNR and magnetic field homogeneity assessment was performed (with a phantom that has the same loading effects as the tissue) to ensure consistent performance from scan to scan. The magnet was shimmed initially using the autoshim routine provided by the manufacturer, followed by manual adjustment of linear and Z^2 shims.

In order to investigate if repeated administration of Gd to the animals (as was done in this study) is neurotoxic, we (1) administered Gd on days 3, 5, 7, 10, 14, 21, and 28 post-SCI to a separate group of 15 injured animals and (2) administered saline on days 3, 5, 7, 10, 14, 21, and 28 post-SCI to a another group of 10 injured animals, using the same protocol for intravascular delivery employed in this study. The BBB locomotor scores were evaluated in both groups of animals.

Animals underwent the DCE-MRI scans on days 3, 7, 14, 28, 42, and 56 post-SCI. In order to reduce mortality, at the recommendation of the veterinarian, MRI scans were not performed on some of the days for certain animals. Significant mortality was observed in animals that were scanned 3 days post-SCI; therefore, the majority of animals that were scanned on day 3 post-SCI were not scanned on subsequent days. Table 1 summarizes the animals that were scanned at each time point. Prior to MRI scans, open field BBB locomotor assessments (23) were performed by two independent observers and BBB scores are reported as the average of those two scores.

Mathematical Model of Gadolinium Distribution in the Rat Spinal Cord

The model for analyzing the DCE-MRI data in rat spinal cord was described previously (19). The concentration of Gd in the extravascular extracellular space (EES), $[Gd(t)_{EES}]$, at each time, *t*, was estimated according to the following formula (19):

$$\left[\mathrm{Gd}(t)_{\mathrm{EES}}\right] = \frac{\mathrm{RIE}(t)}{\mathrm{T}_{10} \times \mathrm{r}_1} \quad (1)$$

where T_{10} is the longitudinal T1 relaxation time prior to administration of Gd, r_1 is the relaxivity, and $\mathrm{RIE}(t) = \frac{\mathrm{S}(t) - \mathrm{S}(0)}{\mathrm{S}(0)}$, where $S(t)$ is the MRI signal intensity at time *t* and *t*=0

denotes the value of the signal prior to injection of the contrast agent. The following values were used: T_{10} = 1.6 s and r_1 = 3.9 $s^{-1}mM^{-1}$ (4,19,25). The value of T_{10} was measured at 7 T on a separate group of animals in a different study (P. A. Narayana, unpublished report). The value of r_1 for Gd has not been reported at 7 T at 37 °C. However, Pintaske et al. (26) have reported a value of 3.9 $s^{-1}mM^{-1}$ for r_1 for Gd in human blood serum at 37 °C at both 1.5 T and 3 T. Therefore, we have used this value in the current studies. As shown previously (25), the rate constants are relatively insensitive to the choice of T_{10} and r_1.

For estimation of the transport coefficients of Gd leakage through compromised BSCB, we considered two compartments: systemic circulation (intravascular) and the EES within the spinal cord. The adequacy of a two-compartment model in spinal cord has been demonstrated in (4,25). The rate of change of Gd(*t*) can be expressed as:

$$\frac{d}{dt}\left[\mathrm{Gd}(t)_{\mathrm{EES}}\right]=\mathrm{K_{ps}}\times\left[\mathrm{Gd}(t)_{\mathrm{P}}\right]-\mathrm{K_{sp}}\times\left(\frac{\mathrm{Gd}(t)_{\mathrm{EES}}}{\mathrm{V}_e}\right) \quad (2)$$

where $\mathrm{Gd}(t)_{\mathrm{EES}}$ and $\mathrm{Gd}(t)_{\mathrm{P}}$ are the concentrations of Gd at time t in the EES and the systemic circulation, respectively, and V_e is a dimensionless parameter that represents the volume fraction of the EES. The parameters K_{ps} and K_{sp} represent the transfer rates of Gd from systemic circulation to the EES compartment and from EES to systemic circulation, respectively. It has been shown that K_{ps} and K_{sp} are unequal (19). For the concentration of Gd in the arterial systemic circulation, we used the empirical formula previously described (19):

$$\left[\mathrm{Gd}(t)_{\mathrm{P}}\right]=\mathrm{A}\times\left(0.4e^{-0.6t}+0.16e^{-0.04t}\right) \quad (3)$$

where A is a constant that is subject-dependent and can be absorbed into the rate constant, K_{ps}. Therefore, without loss of generality we set A = 1. Similarly, the volume fraction of EES, V_e, was also set to unity and absorbed into the rate constant, K_{sp}. With these simplifications, K_{ps} and K_{sp} represent the apparent transfer rate constants and indirectly reflect the status of BSCB permeability. Combining Eqs. 1 and 3 and solving Eq. 2 yields:

$$\left[\mathrm{Gd}(t)_{\mathrm{EES}}\right]=\mathrm{K_{ps}}\times\left(\left(\frac{0.4}{0.6-\mathrm{K_{sp}}}+\frac{0.16}{0.04-\mathrm{K_{sp}}}\right)e^{-\mathrm{K_{sp}}t}\left(\frac{0.4}{0.6-\mathrm{K_{sp}}}\right)e^{-0.6t}-\left(\frac{0.16}{0.04-\mathrm{K_{sp}}}\right)e^{-0.04t}\right) \quad (4)$$

The values of $\mathrm{Gd}(t)_{\mathrm{EES}}$ at each time point were estimated using the DCE-MRI data. These values were fitted to Eq. 4 using Matlab (MathWorks, Inc., Natick, MA) to estimate K_{ps} and K_{sp}. Because of the uncertainty in the exact time of Gd injection and because it improved the ability of the model to fit the data, the time of contrast injection (t_0) was also estimated as a part of the curve fitting routine.

Tissue processing and histology

To verify the K_{ps} results based on DCE-MRI, we used immunohistochemistry (IHC) to detect albumin extravasation into the spinal cord parenchyma. Previous studies have directly (8,27) or indirectly (28) assessed albumin extravasation as an indicator of BSCB integrity in rodent models of spinal cord injury.

Following the terminal MRI scans on day 56 post-SCI, three SCI animals and one uninjured animal were transcardially perfused with saline followed by 4% paraformaldehyde (PFA) in PBS. The spinal cord was then removed, postfixed overnight in 4% PFA, and immersed in

30% sucrose-PBS (0.1 M PBS) for 2-3 days at 4°C. Spinal cords were sectioned into three segments of 3 mm length each: an epicenter segment (centered around the lesion site), a rostral segment, and a caudal segment. Each segment was embedded in tissue freezing medium and frozen at -20°C. Spinal cord segments were sectioned at 35 μm using a cryostat (Leica CM1800, Bannockburn, IL) and stored at -20°C in tissue storing media.

Spinal cord sections were washed three times in 1× PBS for 10 min per wash. Sections were then blocked in 5% goat serum (Invitrogen, Carlsbad, CA) in 1% PBS containing 0.3% Triton X-100 (Sigma, St. Louis, MO) (PBST) for one hour at room temperature. Sections were incubated in the dark in primary antibody (diluted in PBST) for two hours at room temperature. The primary antibody was sheep polyclonal anti-rat albumin fluorescein-5-isothiocyanate (FITC, 1:500, Abcam #ab53435, Cambridge, MA). Sections were washed three times in the dark in 1× PBS for 10 min per wash. Sections were then mounted onto non-subbed slides (Fisher Scientific Company # 12-550-16A, Pittsburgh, PA) and allowed to dry in the dark overnight. Coverslips (Corning Inc. #2940-225, Lowell, MA) were affixed with Fluormount-G (Southern Biotechnology Associates, Inc., Birmingham, AL) prior to visualization.

Tissue sections were viewed and captured using a Spot Flex digital camera (Diagnostic Instruments, Inc., Sterling Heights, MI) attached to a Leica RX1500 upright microscope (Leica Microsystems, Inc., Bannockburn, IL). The albumin antibody was excited at 495 nm and visualized at 520 nm (green visible light). 10x and 20x fluorescence images were captured with SPOT Advanced imaging software (Diagnostic Instruments, Inc., Sterling Heights, MI). For comparisons between sections, the exposure time was held constant for a given magnification level. The primary antibody in one set of spinal cord sections (negative control) was omitted to confirm that the observed signal in the other spinal cord sections that were exposed to the primary antibody is from albumin.

Data Analysis

Exclusion Criteria—Data were excluded if the rat died during the 56 day period subsequent to an observable illness (bloody urine, lack of appetite, reddish porphyrin rings around eyes, etc.). However, if an otherwise healthy rat died after the completion of the MRI scan, the corresponding data was not excluded.

Estimation of NE area—As indicated earlier, three different types of tissues, based on their enhancement behavior, were identified: 1) FE that reflects new vessels which are leaky (4), 2) DE that reflects disrupted vasculature as a result of the initial mechanical trauma, and 3) NE that reflects no visible enhancement. Based on histology, it has been previously shown that FE areas on post-contrast DCE-MR images of injured spinal cord correspond to neovasculature (4,10). The enhancing (FE and DE) areas were identified in an unbiased manner using the statistical decision mechanism that is based on histogram analysis as described elsewhere (4). The NE areas were obtained by subtracting the FE and DE areas from the total spinal cord cross-section. In the event that no enhancing areas were present, the total spinal cord cross-section was considered as the NE area. A typical example of T1-weighted MR images showing DE, FE and NE spinal cord tissue areas is shown in Figure 1. The images shown in this figure were acquired at different sections and on different days for clear visualization of the three different tissue types. As can be seen from this figure, and consistent with previous observations (4), CSF shows enhancement following the administration of Gd. This enhancement is unrelated to the pathology (4).

Estimation of the BSCB permeability (transport) coefficients—The ROI data were analyzed to determine K_{ps} and K_{sp}. Even though we have determined both K_{ps} and K_{sp}, we have focused only on K_{ps} since this parameter is the one that represents leakage of Gd from

the systemic circulation and thus represents the barrier permeability. In addition, K_{sp} tends to be noisy since it is determined from the late time points of the time-concentration curves (25).

Statistics—All statistical analyses were performed using STATA (Intercooled Stata 9.2 for Windows, StataCorp LP, College Station, TX). Generalized estimating equations (GEEs) were used to analyze the longitudinal data. In order to determine the overall association between the BBB scores and K_{ps} values we used the GEE procedure for a population-averaged model (29). The GEE procedure allowed us to test the significance of the relationship between two major outcome variables (BBB scores and K_{ps} values in NE areas) while simultaneously accounting for the correlation among the temporally repeated observations for each animal. Unlike multiple analyses of variance (MANOVA) which requires the imputation of missing data by using options such as last value carried forward, longitudinal interpolation, longitudinal regression, etc., GEE can handle cases with missing data without the need for imputation (30). Using various imputation methods on an incomplete longitudinal dataset, Twisk et al. (30) concluded that not imputing missing data would result in superior GEE results, while imputing missing data would result in superior MANOVA results. Because any imputation technique introduces some bias, we chose not to impute any missing data and employed GEE analysis.

All values are reported as mean ± standard deviation unless otherwise stated. Statistical significance was defined as $p<0.05$, with corrections for multiple comparisons affecting the cutoff value, α, against which the measured p-value is compared (Bonferroni adjustment). To attain statistical significance, the p-value must have been less than or equal to the value of α corrected for multiple comparisons.

RESULTS

The BBB scores of two different injured cohorts that received Gd (n=15) and saline (n=10) at multiple time points are shown in Figure 2. There was no statistical difference in the BBB scores between the SCI animals receiving Gd or saline. Thus this experiment suggests that chronic administration of Gd in SCI animals has no significant effect on neurobehavioral scores. In addition, the mortality between these two cohorts was not different.

About 70% of the animals planned for 56-day study (n=10) survived until this time point. Some of the reasons for mortality in this cohort included suspected kidney failure at 45d post-SCI (animal 2), development of a sore due to immobility at 46d post-SCI (animal 13), and respiratory infection at 51d post-SCI (animal 11). These three animals were sacrificed prior to their last scheduled scan at the recommendation of the veterinarian.

The BSCB permeability parameters were calculated on days 3, 7, 14, 28, 42, and 56 post-injury. In addition to comparing the values of K_{ps} by individual days, data was also analyzed by three post-SCI time periods: acute (day 3), subacute (between days 7 and 14), and chronic (after day 14). Additionally, the spatial locations were grouped into three regions: caudal region (slices that were 4-8mm caudal to the injury epicenter), epicenter region (slices that were $\leq$ 2mm away from the injury epicenter (including the epicenter slice itself)), and rostral region (slices that were 4-8mm rostral to the injury epicenter).

For each scan, the SCI epicenter on MRI was determined independently by two observers as the slice with the largest lesion. If the observers' choice of epicenter slice did not match, they conferred until an epicenter slice was agreed upon.

BSCB permeability in uninjured spinal cord

In uninjured animals, the value of K_{ps} was too small to measure because of the intact barrier. Therefore, we calculated the baseline K_{ps} from slices which were ≥10mm rostral to the epicenter of injury. This value was found to be 0.006978±0.001864 min^{-1}. As can be seen in Table 2, this baseline value of K_{ps} is significantly smaller than the values of K_{ps} in NE areas at all spatial regions and at all time periods (unpaired two-tailed Student t-test).

BSCB permeability in non-enhancing tissue

Figure 3 shows the spatial variation of K_{ps} along the length of the spinal cord for different post-SCI time periods. In this plot, each data point represents the value of K_{ps} for each 1mm slice of the spinal cord relative to the epicenter of injury. In the acute period (Figure 3a) a caudalrostral asymmetry in the BSCB permeability, with a leakier BSCB (corresponding to greater K_{ps} values) caudally than rostrally, was observed (two-tailed Student t-test: $p \leq 0.0028$). This asymmetry was not statistically significant in the subacute and chronic phases. We initially considered whether the values of K_{ps} changed significantly between successive scan days. Because no significant differences were detected in adjacent-day comparisons, the analysis was repeated between pairs of the three time periods (α corrected for multiple comparisons = 0.0167). As can be seen in Figure 4, K_{ps} was significantly greater in the acute period compared to both the subacute and chronic periods.

The values of K_{ps} within each spatial region were then tested for significant changes over time (α corrected for multiple comparisons = 0.0167). As can be seen in Figure 5, K_{ps} in the caudal region was significantly smaller in the subacute and chronic periods compared to in the acute time period. In the epicenter region, K_{ps} was significantly smaller in the chronic period compared to in the acute period.

BSCB permeability in enhancing tissue

Figure 6 displays the value of K_{ps} in NE and FE tissue areas, over time. In both tissue areas, K_{ps} decreased with time, with the value of K_{ps} in FE areas being consistently greater than that in NE areas for each time period. Despite the variance in the K_{ps} data, significant differences based on time post-SCI and spatial region were detected, even after correcting for multiple comparisons. As pointed out in this manuscript and in the published literature (4), relatively few focal enhancements are seen in the acute or subacute periods.

Relationship between BBB scores and BSCB permeability

The relationship between BBB scores and K_{ps} values in NE areas was tested (α corrected for multiple comparisons = 0.01) and the results are shown in Figure 7. The overall association between these two outcomes (BBB scores and K_{ps} values in NE areas) was statistically significant ($p<0.001$). Next, the association between K_{ps} and BBB score was tested in each of the three spatial regions of the spinal cord. The association between K_{ps} and BBB score was statistically significant ($p<0.001$) in all three spatial regions (denoted by "**" in the legend of Figure 7).

In order to determine which spatial region(s) contributed most to the overall association between K_{ps} and BBB scores, the GEE procedure was performed to test for interactions between BBB scores and K_{ps} values within each of the three spatial regions in the spinal cord. A significant interaction between the epicenter region and the BBB score was found ($p<0.001$, α corrected for multiple comparisons = 0.01). Table 3 summarizes the statistically significant results for overall association, region-specific association, and region-specific interaction between BBB scores and BSCB permeability parameter K_{ps} in NE areas.

Qualitative histological verification of DCE-MRI results

Histology was evaluated qualitatively. As shown in Figure 8, albumin staining was prominent in the epicenter region/segment, in both the injured tissue area (dorsal spinal cord) and the uninjured area (ventral spinal cord) that appears as a NE area on DCE-MRI. In the caudal region/segment, albumin extravasation persisted in the NE area (ventral spinal cord), confirming that the BSCB is not fully restored by this time point. The albumin staining in the uninjured control spinal cord was similar to that observed for the negative control sections that were not treated with the primary antibody (data not shown).

DISCUSSION

We have non-invasively investigated both the temporal and spatial evolution of BSCB permeability in the non-enhancing tissue on post-contrast images with DCE-MRI. We investigated the temporal changes in BSCB permeability over a period of eight weeks post-injury. We believe this is the longest post-injury period over which changes in BSCB permeability have been investigated. For example, Popovich et al. (11) and Bilgen et al. (25) have previously investigated the temporal changes in BSCB permeability up to 28d post-injury.

In order to assure robustness of the data in these longitudinal studies, we have implemented a rigorous quality assurance program that minimizes changes in SNR and shim settings from one scan to the next. In addition, our measurements of K_{ps} are based on normalization of post-contrast signal intensity to pre-contrast signal intensity. Therefore the estimation of the transfer coefficients at different time points is expected to be quite stable.

Our studies show that the BSCB permeability gradually reduced with post-SCI time, but that the BSCB remains compromised even at eight weeks post-injury. The gradual reduction of BSCB permeability could be one of the endogenous repair processes that have been well documented; see for example, (10).

Popovich et al. (11) have shown that the BSCB is compromised for as long as 28 days post-SCI and is completely restored thereafter. Whetstone et al. (18) have observed restoration of the BSCB between 7-14d post-injury. In contrast, our studies show that the barrier remains compromised even at 56d post-injury based on both DCE-MRI analysis (Figure 5) and IHC (Figure 8). This is confirmed by our IHC results demonstrating extravasation of albumin. Our DCE-MRI studies, consistent with histology-based studies (11,17,18) as well as our own histology results described above, demonstrate that tissues that are as far as 8mm rostral and caudal to the site of injury are compromised.

One of the important observations made in these studies is the inverse correlation between BSCB permeability and the BBB scores. A statistically significant association between the BSCB permeability parameter K*ps* and BBB locomotor score was observed. Not only was the association between K_{ps} and BBB score significant overall ($p<0.001$), but it was also significant in each of the three spatial regions ($p<0.001$ in each region). A significant interaction between K_{ps} and BBB score ($p<0.001$) was found in the epicenter region.

Our studies suggest a correlation between the restoration of BSCB and locomotor recovery post-SCI. A number of mechanisms could contribute to this observed correlation. For example, reduced extravasation of agents from the systemic vasculature (e.g. plasma proteins, immune cells) have been shown to exacerbate SCI through downstream mechanisms of edema and reactive oxygen species (34-40). Attenuation of edema and nitric oxide synthase expression (which is involved in the formation of reactive oxygen species) post-SCI has been attributed to improvements post-SCI (41-44). Therefore, we believe that restoration of BSCB limits the entry of many of the neurotoxins into the spinal cord parenchyma. Based on these results we

also hypothesize that vascular stabilizing agents such as angiopoietin-1 could further improve the outcome (31,45-47).

An asymmetry was found at 3d post-SCI in that BSCB permeability, as quantified by the K_{ps} parameter, was greater caudal to than rostral to the epicenter of injury. Like increased BSCB permeability, oxidative stress represents another process of the secondary sequelae of SCI. Baldwin et al. (48) showed a similar asymmetric pattern in the staining of 4-hydroxynonenal/protein complex (HNE), a marker of lipid peroxidation and oxidative stress, in a rat model of T10 contusion SCI. They found increased HNE staining caudally compared to rostrally, at 2d post-SCI.

While the BSCB permeability was significantly reduced over time in the caudal and epicenter regions, a similar change was not detected in the rostral region (see Figure 5). These results parallel the MRI and histological studies described by Narayana et al. (10), who found that neuronal recovery was more pronounced caudal to than rostral to the injury epicenter. Based on Nissl and immunofluorescence staining, Narayana et al. (10) observed larger cavities and increased disruption in spinal cord grey matter in regions rostral to the injury epicenter. Those findings, combined with our present findings, suggest that delayed reconstitution of the BSCB rostrally may impede endogenous recovery processes post-SCI in this region of the spinal cord.

Our studies differ from the earlier published studies by Bilgen et al. (4,19) in a number of ways: 1) our studies focus on the NE regions, 2) we have retained the spatial information of the BSCB permeability, 3) we have extended these experiments to 56 days post-injury, 4) these studies were performed at 7T magnetic field strength, which offers a superior signal-to-noise ratio (SNR) that was exploited to improve the spatial resolution (1mm slice thickness), and 5) we have correlated the BSCB permeability with neurobehavioral studies as assessed by the Basso-Beattie-Bresnahan (BBB) score (23), the most commonly used instrument in SCI.

Recent studies by Nesic et al. (49) and Gordh et al. (27) implicated compromised BSCB in neuropathic pain. Thus it would have been interesting to correlate BSCB permeability with neurosensory measures. Unfortunately we did not include neurosensory measures that objectively measure neuropathic pain. In future studies, we plan to include measures such as the von Frey hair filament test, which measures the mechanical allodynia experienced after SCI (50,51).

Because of the animal mortality in these longitudinal studies, not every animal was scanned at each time point. A number of factors could have contributed to the animal mortality in the current studies. For example, isoflurane dose used in these studies could predispose animals to neurogenic pulmonary edema (52-55). The mortality that we observed in our laboratory is comparable to that observed in other SCI laboratories, employing the same breed of rats and at the same injury severity, where animals are not subjected to repeated anesthesia (Raymond Grill, Ph.D., personal communication). Therefore, it is perhaps unlikely that isoflurane-induced neurogenic pulmonary edema was the culprit. However, we can not rule out endothelial damage in these rats. Another possible confounder is the repeated application of Gd in a condition where increased BSCB permeability may lead to further tissue damage. However, this does not appear to be the case since our other experiment showed no statistically significant differences in the BBB scores between two other SCI cohorts that were subjected to chronic Gd and saline administration (see Figure 2).

CONCLUSIONS

We have non-invasively determined the temporal and spatial changes in BSCB permeability in experimental SCI by analyzing DCE-MRI studies using a two-compartment pharmacokinetic model. A decrease in BSCB permeability with increasing distance (both

rostrally and caudally) from the epicenter of the injury was observed. A gradual restoration of the barrier with post-injury time was also observed. However, based on DCE-MRI, and confirmed by immunohistochemistry, the BSCB remained compromised distal to the SCI epicenter, even 56d post-SCI. These studies also demonstrate a significant inverse correlation between the BSCB permeability and neuromotor recovery in the post-injury period.

ACKNOWLEDGEMENTS

These studies are supported by NIH/NINDS (Grant # NS045624) to PAN. The 7T MRI scanner is funded by NIH/NCRR (Grant # S10 RR17205-01) under the High End Instrumentation Program (PAN). We thank Chul Ahn, Ph.D. for expert statistical advice and Juan Herrera, Ph.D. for help with immunohistochemistry.

List of abbreviations used

BBB, (Basso-Beattie-Bresnahan)
BSCB, (blood-spinal cord barrier)
CNS, (central nervous system)
DCE-MRI, (dynamic contrast-enhanced MRI)
DE, (diffuse enhancement)
EES, (extravascular extracellular space)
FE, (focal enhancement)
Gd, (gadopentate dimeglumine)
GEE, (generalized estimating equation)
GM, (grey matter)
IHC, (immunohistochemistry)
NE, (non-enhancing)
PBS, (phosphate buffered saline)
PBST, (PBS containing Triton X-100)
PFA, (paraformaldehyde)
RF, (radiofrequency)
ROI, (region of interest)
SNR, (signal-to-noise ratio)
WM, (white matter)

REFERENCES

1. Rossignol S, Schwab M, Schwartz M, Fehlings MG. Spinal cord injury: time to move? J Neurosci 2007;27:11782–92. [PubMed: 17978014]
2. Tator CH. Biology of neurological recovery and functional restoration after spinal cord injury. Neurosurgery 1998;42:696–707. [PubMed: 9574633]discussion 707-8
3. Young W. Secondary injury mechanisms in acute spinal cord injury. J Emerg Med 1993;11(Suppl 1): 13–22. [PubMed: 8445198]
4. Bilgen M, Abbe R, Narayana PA. Dynamic contrast-enhanced MRI of experimental spinal cord injury: in vivo serial studies. Magn Reson Med 2001;45:614–22. [PubMed: 11283989]
5. Blight AR. Morphometric analysis of a model of spinal cord injury in guinea pigs, with behavioral evidence of delayed secondary pathology. J Neurol Sci 1991;103:156–71. [PubMed: 1880533]
6. Casella GT, Marcillo A, Bunge MB, Wood PM. New vascular tissue rapidly replaces neural parenchyma and vessels destroyed by a contusion injury to the rat spinal cord. Exp Neurol 2002;173:63–76. [PubMed: 11771939]
7. Loy DN, Crawford CH, Darnall JB, Burke DA, Onifer SM, Whittemore SR. Temporal progression of angiogenesis and basal lamina deposition after contusive spinal cord injury in the adult rat. J Comp Neurol 2002;445:308–24. [PubMed: 11920709]
8. Maikos JT, Shreiber DI. Immediate damage to the blood-spinal cord barrier due to mechanical trauma. J Neurotrauma 2007;24:492–507. [PubMed: 17402855]

9. Mautes AE, Weinzierl MR, Donovan F, Noble LJ. Vascular events after spinal cord injury: contribution to secondary pathogenesis. Phys Ther 2000;80:673–87. [PubMed: 10869130]
10. Narayana PA, Grill RJ, Chacko T, Vang R. Endogenous recovery of injured spinal cord: longitudinal in vivo magnetic resonance imaging. J Neurosci Res 2004;78:749–59. [PubMed: 15499591]
11. Popovich PG, Horner PJ, Mullin BB, Stokes BT. A quantitative spatial analysis of the blood-spinal cord barrier. I. Permeability changes after experimental spinal contusion injury. Exp Neurol 1996;142:258–75. [PubMed: 8934558]
12. Shingu H, Kimura I, Nasu Y, Shiotani A, Oh-hama M, Hijioka A, Tanaka J. Microangiographic study of spinal cord injury and myelopathy. Paraplegia 1989;27:182–9. [PubMed: 2762005]
13. Tator CH, Koyanagi I. Vascular mechanisms in the pathophysiology of human spinal cord injury. J Neurosurg 1997;86:483–92. [PubMed: 9046306]
14. Westergren H, Farooque M, Olsson Y, Holtz A. Spinal cord blood flow changes following systemic hypothermia and spinal cord compression injury: an experimental study in the rat using Laser-Doppler flowmetry. Spinal Cord 2001;39:74–84. [PubMed: 11402362]
15. Davson, H. An Introduction to the Blood-Brain Barrier. Vol. vol. 7. CRC Press; Boca Raton: 1993. p. 335
16. Pardridge, WM. The Blood-Brain Barrier: Cellular and Molecular Biology. Vol. vol. xix. Raven Press; New York City: 1993. p. 476
17. Noble LJ, Wrathall JR. Distribution and time course of protein extravasation in the rat spinal cord after contusive injury. Brain Res 1989;482:57–66. [PubMed: 2706482]
18. Whetstone WD, Hsu JY, Eisenberg M, Werb Z, Noble-Haeusslein LJ. Blood-spinal cord barrier after spinal cord injury: relation to revascularization and wound healing. J Neurosci Res 2003;74:227–39. [PubMed: 14515352]
19. Bilgen M, Narayana PA. A pharmacokinetic model for quantitative evaluation of spinal cord injury with dynamic contrast-enhanced magnetic resonance imaging. Magn Reson Med 2001;46:1099–106. [PubMed: 11746575]
20. Runge VM, Wells JW, Baldwin SA, Scheff SW, Blades DA. Evaluation of the temporal evolution of acute spinal cord injury. Invest Radiol 1997;32:105–10. [PubMed: 9039583]
21. Tofts PS, Brix G, Buckley DL, Evelhoch JL, Henderson E, Knopp MV, Larsson HB, Lee TY, Mayr NA, Parker GJ, Port RE, Taylor J, Weisskoff RM. Estimating kinetic parameters from dynamic contrast-enhanced T(1)-weighted MRI of a diffusable tracer: standardized quantities and symbols. J Magn Reson Imaging 1999;10:223–32. [PubMed: 10508281]
22. Tarlov IM. Spinal cord compression studies. III. Time limits for recovery after gradual compression in dogs. AMA Arch Neurol Psychiatry 1954;71:588–97.
23. Basso DM, Beattie MS, Bresnahan JC. A sensitive and reliable locomotor rating scale for open field testing in rats. J Neurotrauma 1995;12:1–21. [PubMed: 7783230]
24. Fenyes DA, Narayana PA. In vivo echo-planar imaging of rat spinal cord. Magn Reson Imaging 1998;16:1249–55. [PubMed: 9858282]
25. Bilgen M, Dogan B, Narayana PA. In vivo assessment of blood-spinal cord barrier permeability: serial dynamic contrast enhanced MRI of spinal cord injury. Magn Reson Imaging 2002;20:337–41. [PubMed: 12165352]
26. Pintaske J, Martirosian P, Graf H, Erb G, Lodemann KP, Claussen CD, Schick F. Relaxivity of Gadopentetate Dimeglumine (Magnevist), Gadobutrol (Gadovist), and Gadobenate Dimeglumine (MultiHance) in human blood plasma at 0.2, 1.5, and 3 Tesla.(erratum appears in Invest Radiol. 2006 Dec;41(12):859). Investigative Radiology 2006;41:213–21. [PubMed: 16481903]
27. Gordh T, Chu H, Sharma HS. Spinal nerve lesion alters blood-spinal cord barrier function and activates astrocytes in the rat. Pain 2006;124:211–21. [PubMed: 16806707]
28. Sharma HS, Skottner A, Lundstedt T, Flardh M, Wiklund L. Neuroprotective effects of melanocortins in experimental spinal cord injury. An experimental study in the rat using topical application of compounds with varying affinity to melanocortin receptors. J Neural Transm 2006;113:463–76. [PubMed: 16550325]
29. Zeger SL, Liang KY, Albert PS. Models for longitudinal data: a generalized estimating equation approach. Biometrics 1988;44:1049–60. [PubMed: 3233245]

30. Twisk J, de Vente W. Attrition in longitudinal studies. How to deal with missing data. J Clin Epidemiol 2002;55:329–37. [PubMed: 11927199]

31. Thurston G, Rudge JS, Ioffe E, Zhou H, Ross L, Croll SD, Glazer N, Holash J, McDonald DM, Yancopoulos GD. Angiopoietin-1 protects the adult vasculature against plasma leakage. Nat Med 2000;6:460–3. [PubMed: 10742156]

32. Zacharek A, Chen J, Cui X, Li A, Li Y, Roberts C, Feng Y, Gao Q, Chopp M. Angiopoietin1/Tie2 and VEGF/Flk1 induced by MSC treatment amplifies angiogenesis and vascular stabilization after stroke. J Cereb Blood Flow Metab 2007;27:1684–91. [PubMed: 17356562]

33. Zhang ZG, Zhang L, Croll SD, Chopp M. Angiopoietin-1 reduces cerebral blood vessel leakage and ischemic lesion volume after focal cerebral embolic ischemia in mice. Neuroscience 2002;113:683–7. [PubMed: 12150788]

34. Bao F, Liu D. Hydroxyl radicals generated in the rat spinal cord at the level produced by impact injury induce cell death by necrosis and apoptosis: protection by a metalloporphyrin. Neuroscience 2004;126:285–95. [PubMed: 15207346]

35. Carlson SL, Parrish ME, Springer JE, Doty K, Dossett L. Acute inflammatory response in spinal cord following impact injury. Exp Neurol 1998;151:77–88. [PubMed: 9582256]

36. Genovese T, Cuzzocrea S. Role of free radicals and poly(ADP-ribose)polymerase-1 in the development of spinal cord injury: new potential therapeutic targets. Curr Med Chem 2008;15:477–87. [PubMed: 18289003]

37. Genovese T, Mazzon E, Crisafulli C, Di Paola R, Muia C, Bramanti P, Cuzzocrea S. Immunomodulatory effects of etanercept in an experimental model of spinal cord injury. J Pharmacol Exp Ther 2006;316:1006–16. [PubMed: 16303916]

38. Genovese T, Mazzon E, Crisafulli C, Esposito E, Di Paola R, Muia C, Di Bella P, Bramanti P, Cuzzocrea S. Effects of combination of melatonin and dexamethasone on secondary injury in an experimental mice model of spinal cord trauma. J Pineal Res 2007;43:140–53. [PubMed: 17645692]

39. Genovese T, Mazzon E, Crisafulli C, Esposito E, Di Paola R, Muia C, Di Bella P, Meli R, Bramanti P, Cuzzocrea S. Combination of dexamethasone and etanercept reduces secondary damage in experimental spinal cord trauma. Neuroscience 2007;150:168–81. [PubMed: 17945432]

40. Xu W, Chi L, Xu R, Ke Y, Luo C, Cai J, Qiu M, Gozal D, Liu R. Increased production of reactive oxygen species contributes to motor neuron death in a compression mouse model of spinal cord injury. Spinal Cord 2005;43:204–13. [PubMed: 15520836]

41. Sharma HS, Nyberg F, Westman J, Alm P, Gordh T, Lindholm D. Brain derived neurotrophic factor and insulin like growth factor-1 attenuate upregulation of nitric oxide synthase and cell injury following trauma to the spinal cord. An immunohistochemical study in the rat. Amino Acids 1998;14:121–9. [PubMed: 9871451]

42. Sharma HS, Westman J, Nyberg F. Topical application of 5-HT antibodies reduces edema and cell changes following trauma of the rat spinal cord. Acta Neurochir Suppl 1997;70:155–8. [PubMed: 9416307]

43. Sharma HS, Winkler T, Stalberg E, Gordh T, Alm P, Westman J. Topical application of TNF-alpha antiserum attenuates spinal cord trauma induced edema formation, microvascular permeability disturbances and cell injury in the rat. Acta Neurochir Suppl 2003;86:407–13. [PubMed: 14753477]

44. Winkler T, Sharma HS, Stalberg E, Badgaiyan RD. Neurotrophic factors attenuate alterations in spinal cord evoked potentials and edema formation following trauma to the rat spinal cord. Acta Neurochir Suppl 2000;76:291–6. [PubMed: 11450028]

45. Suri C, McClain J, Thurston G, McDonald DM, Zhou H, Oldmixon EH, Sato TN, Yancopoulos GD. Increased vascularization in mice overexpressing angiopoietin-1. Science 1998;282:468–71. [PubMed: 9774272]

46. Thurston G, Rudge JS, Ioffe E, Papadopoulos N, Daly C, Vuthoori S, Daly T, Wiegand SJ, Yancopoulos GD. The anti-inflammatory actions of angiopoietin-1. Exs 2005:233–45. [PubMed: 15617482]

47. Thurston G, Suri C, Smith K, McClain J, Sato TN, Yancopoulos GD, McDonald DM. Leakage-resistant blood vessels in mice transgenically overexpressing angiopoietin-1. Science 1999;286:2511–4. [PubMed: 10617467]

48. Baldwin SA, Broderick R, Osbourne D, Waeg G, Blades DA, Scheff SW. The presence of 4-hydroxynonenal/protein complex as an indicator of oxidative stress after experimental spinal cord contusion in a rat model. J Neurosurg 1998;88:874–83. [PubMed: 9576257]

49. Nesic O, Lee J, Johnson KM, Ye Z, Xu GY, Unabia GC, Wood TG, McAdoo DJ, Westlund KN, Hulsebosch CE, Perez-Polo J. Regino. Transcriptional profiling of spinal cord injury-induced central neuropathic pain. J Neurochem 2005;95:998–1014. [PubMed: 16219025]

50. Bryce TN, Budh CN, Cardenas DD, Dijkers M, Felix ER, Finnerup NB, Kennedy P, Lundeberg T, Richards JS, Rintala DH, Siddall P, Widerstrom-Noga E. Pain after spinal cord injury: an evidence-based review for clinical practice and research. Report of the National Institute on Disability and Rehabilitation Research Spinal Cord Injury Measures meeting. J Spinal Cord Med 2007;30:421–40. [PubMed: 18092558]

51. Christensen MD, Everhart AW, Pickelman JT, Hulsebosch CE. Mechanical and thermal allodynia in chronic central pain following spinal cord injury. Pain 1996;68:97–107. [PubMed: 9252004]

52. Kandatsu N, Nan YS, Feng GG, Nishiwaki K, Hirokawa M, Ishikawa K, Komatsu T, Yokochi T, Shimada Y, Ishikawa N. Opposing effects of isoflurane and sevoflurane on neurogenic pulmonary edema development in an animal model. Anesthesiology 2005;102:1182–9. [PubMed: 15915031]

53. Rezaiguia-Delclaux S, Jayr C, Luo DF, Saidi NE, Meignan M, Duvaldestin P. Halothane and isoflurane decrease alveolar epithelial fluid clearance in rats. Anesthesiology 1998;88:751–60. [PubMed: 9523820]

54. Sedy J, Urdzikova L, Likavcanova K, Hejcl A, Burian M, Jendelova P, Zicha J, Kunes J, Sykova E. Low concentration of isoflurane promotes the development of neurogenic pulmonary edema in spinal cord injured rats. J Neurotrauma 2007;24:1487–501. [PubMed: 17892410]

55. Sedy J, Urdzikova L, Likavcanova K, Hejcl A, Jendelova P, Sykova E. A new model of severe neurogenic pulmonary edema in spinal cord injured rat. Neurosci Lett 2007;423:167–71. [PubMed: 17698290]

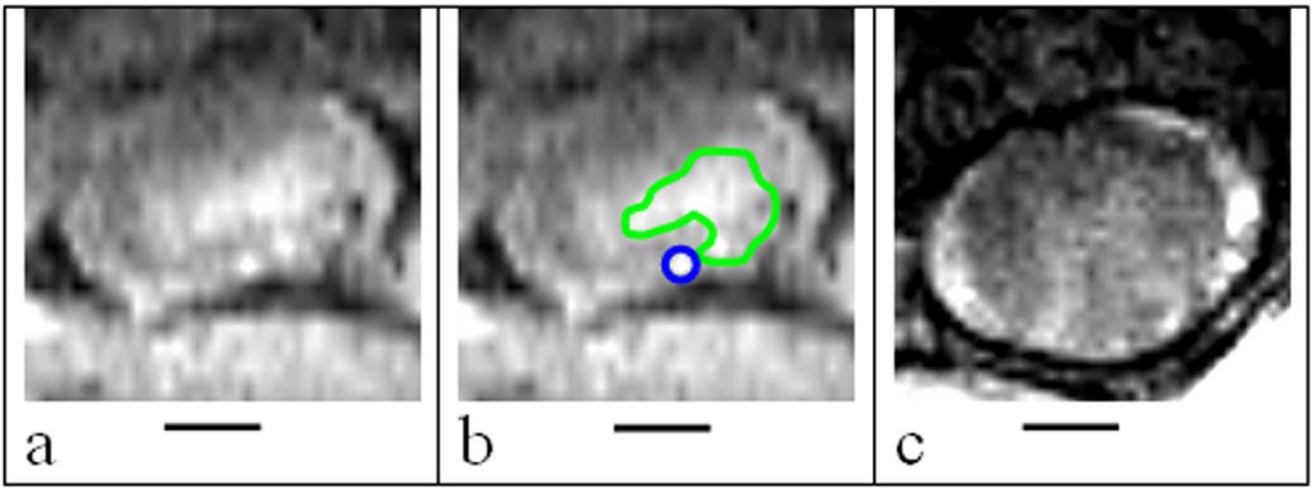

Figure 1.
Representative axial DCE-MR images containing the different areas of interest (FE area is outlined in blue and DE area is outlined in green). The NE area is calculated by subtracting the FE and DE areas from the entire spinal cord ROI. (a) An axial T1-weighted MRI slice of the spinal cord; (b) the same slice as in (a), with DE and FE areas outlined in green and blue respectively; and (c) an example of a slice that contains only NE areas. The hyperintense ring around the spinal cord contains cerebrospinal fluid (4). Bars represent 1 mm.

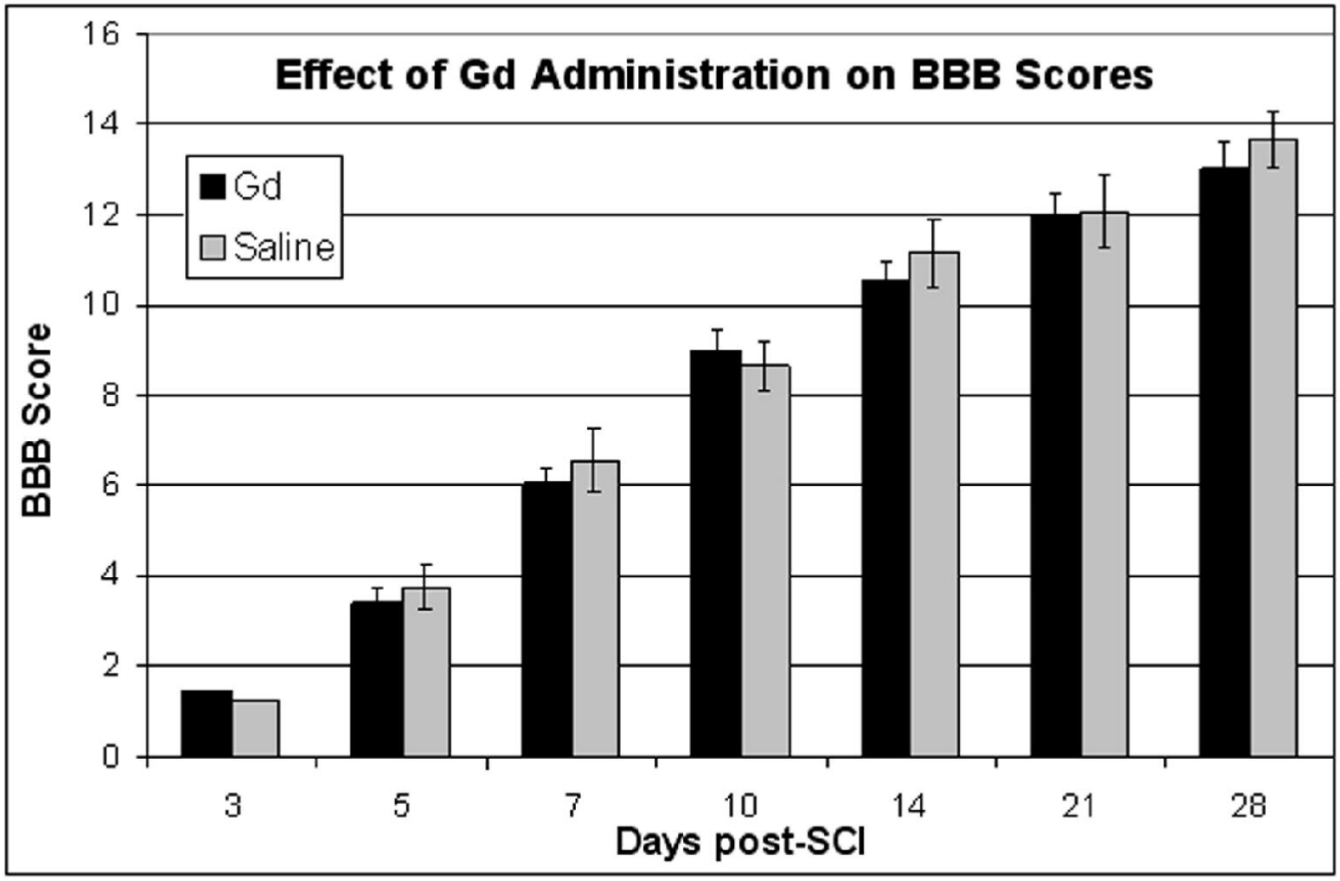

Figure 2.
Effect of chronic administration of Gd or saline on BBB scores in SCI. Error bars represent standard error of the mean.

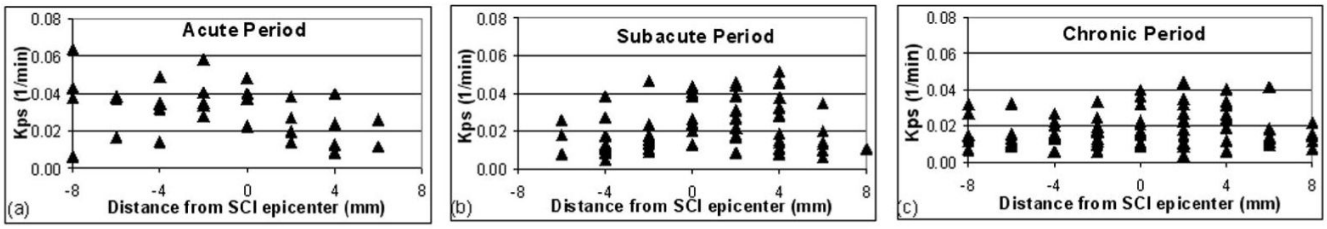

Figure 3.

Variation of K_{ps} in the NE areas along the length of an injured spinal cord for different post-SCI time periods. The distance 0 represents the epicenter. Negative and positive values of distance correspond to locations caudal and rostral to the epicenter of injury, respectively. The acute, subacute, and chronic time periods correspond to post-SCI day 3; days 7 and 14; and days 28, 42, and 56, respectively.

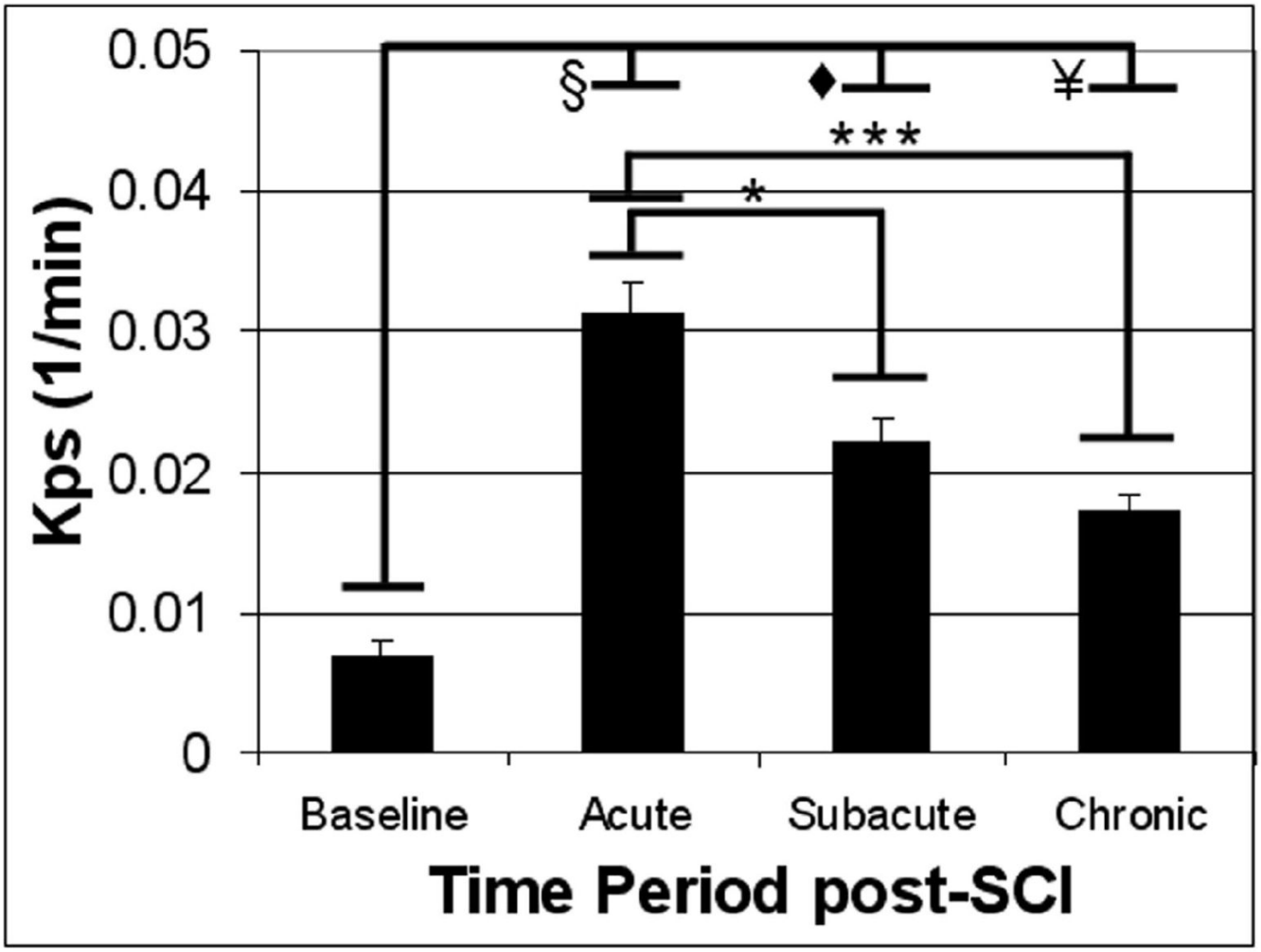

Figure 4.

K_{ps} in the NE areas in the three post-SCI time periods. * indicates $p<0.01$, *** indicates $p<0.0001$, ¥ indicates $p<10^{-5}$, ◆ indicates $p<10^{-8}$, and § indicates $p<10^{-11}$. Error bars represent standard error of the mean.

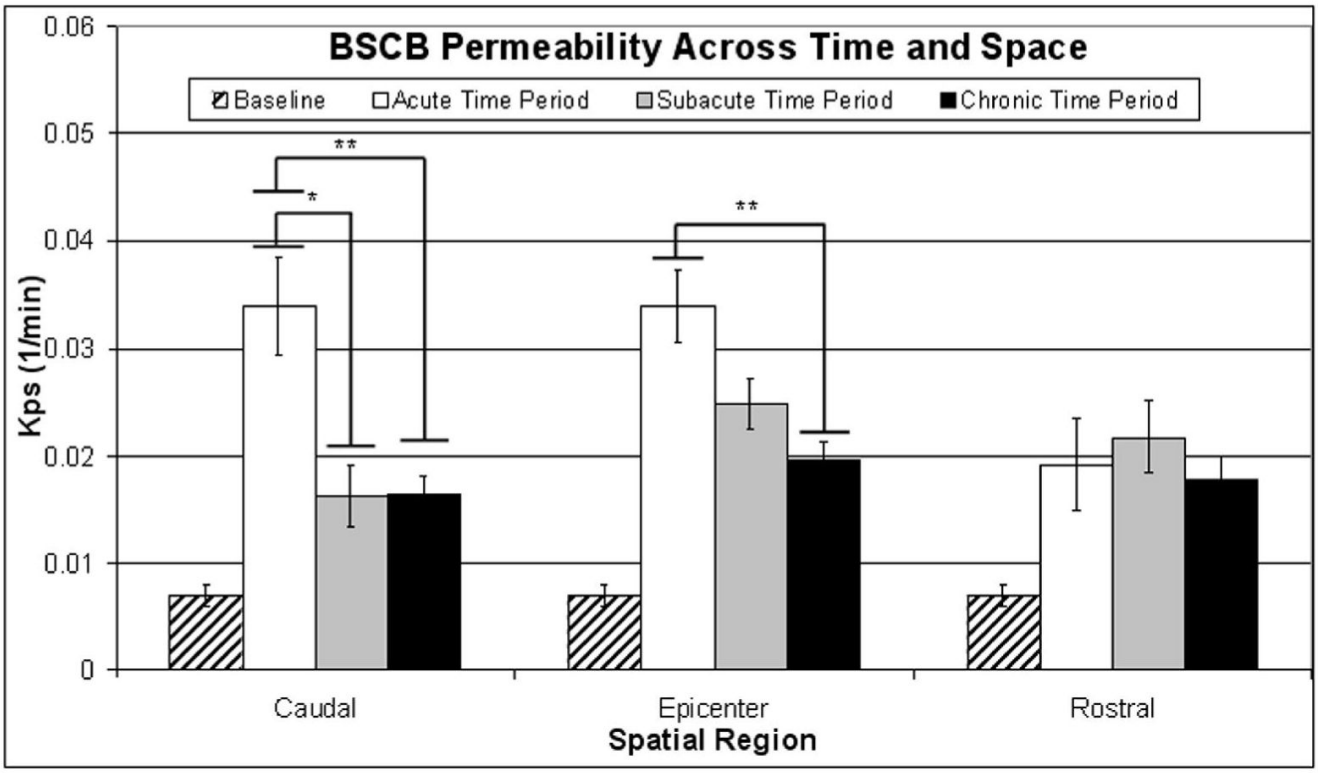

Figure 5.

Variation of K_{ps} in NE areas across time and space. * indicates $p<0.01$ and ** indicates $p<0.001$. Error bars represent standard error of the mean. Statistical differences in K_{ps} between NE areas and baseline values are summarized in Table 2.

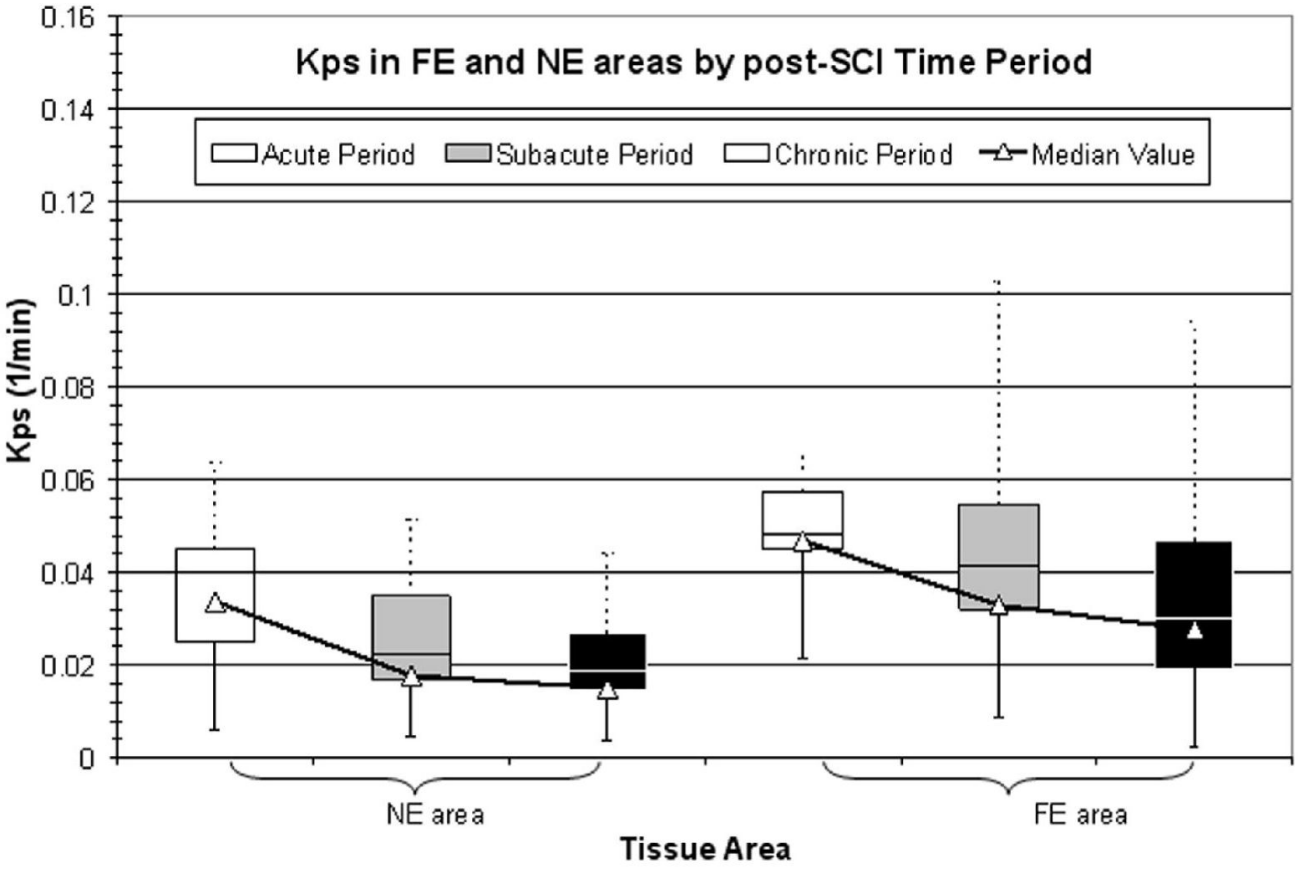

Figure 6.

Variation of K_{ps} in NE and FE areas over time. For a given tissue area in a given time period, the upper box represents the third quartile and the lower box represents the second quartile. The upper (dotted) and lower (solid) bars represent the maximum and minimum values, respectively. The triangles represent the median values.

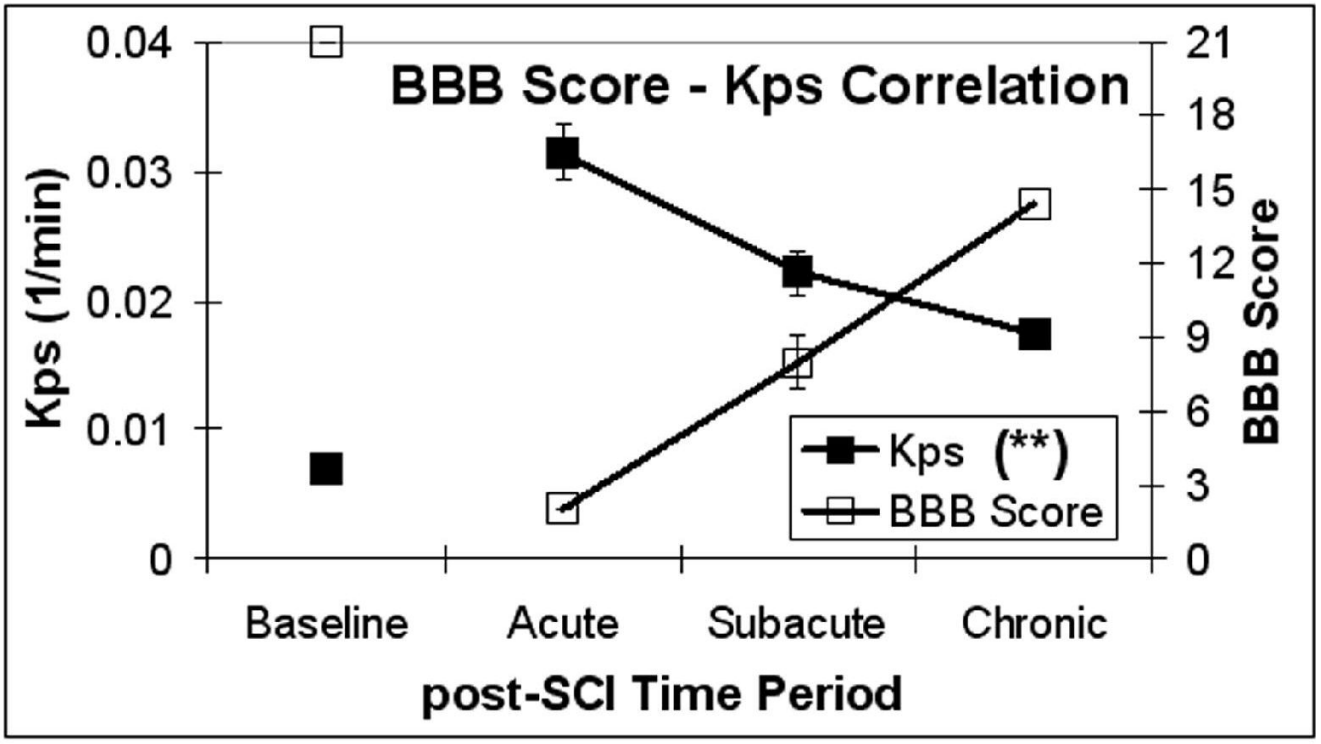

Figure 7.
Variation of K_{ps} in NE areas (solid squares) and the BBB locomotor score (open squares) during the three post-SCI time periods. Statistical significance was seen ($p<0.001$ (**)) for the association between K_{ps} and BBB score. Error bars represent standard error of the mean.

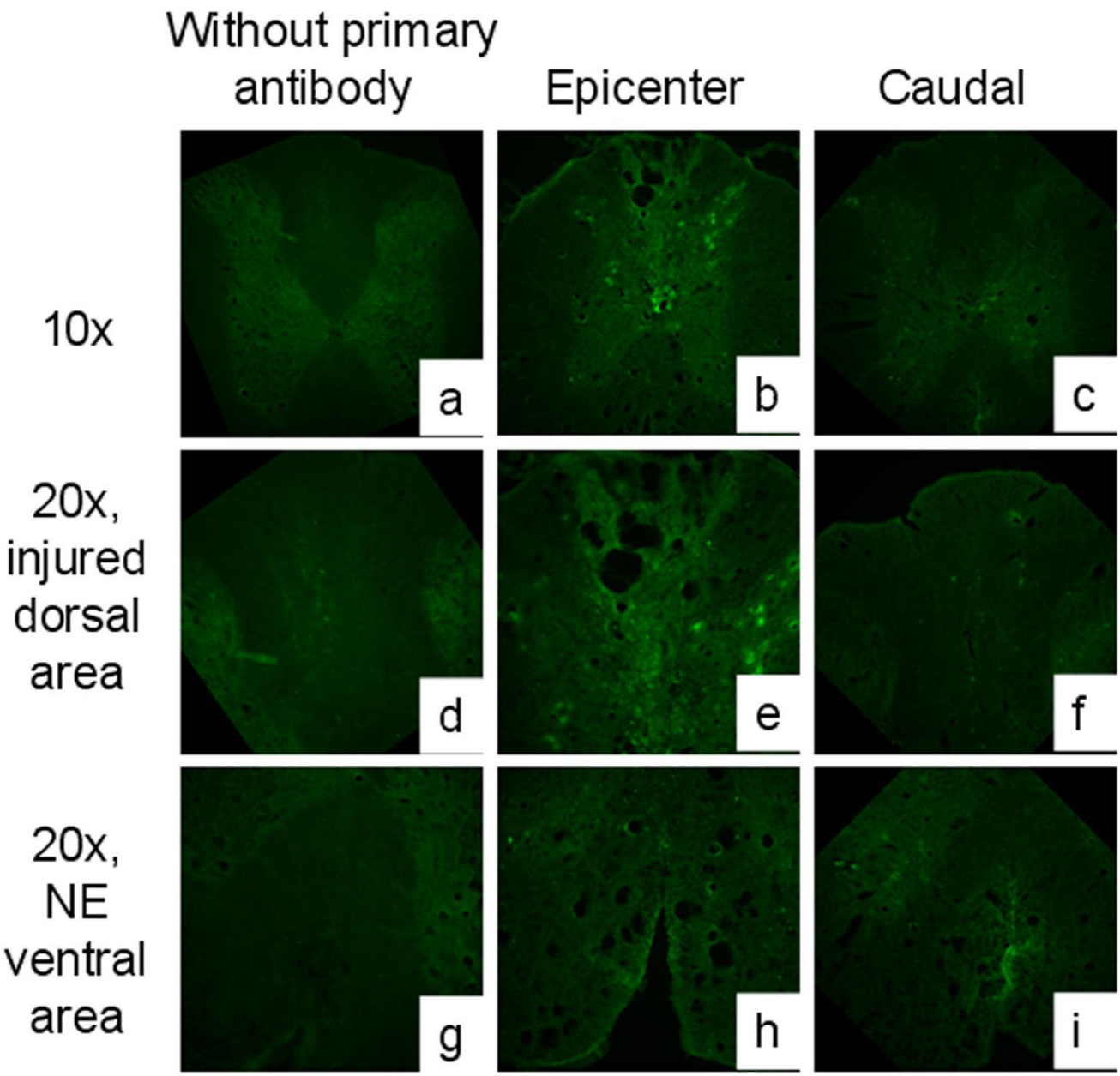

Figure 8.
Albumin extravasation at day 56 post-SCI. The absence of primary antibody (a, d, g) confirms the validity of observed albumin signal. In the epicenter region (b, e, h) there is marked staining for albumin at both the injury site (e) and the NE area (h). In the caudal region (c, f, i) there is less staining compared to epicenter, but albumin extravasation can be seen in the NE area(i).

Table 1

Summary of the animals scanned at the specified post-SCI time points

Days post-SCI:	Day 3	Day 7	Day 14	Day 28	Day 42	Day 56
Animal Number:					1	1
	2	2			2	
		3	3	3	3	
		4	4	4		4
		5	5	5	5	5
		6	6	6	6	6
	7					
	8					
	9					
	10					
		11	11			
			12			
				13		
						14
Total number of animals:	**5**	**6**	**6**	**5**	**5**	**5**

Table 2

Summary of the statistical tests comparing the K_{ps} values between baseline and NE area

Baseline K_{ps} values compared to NE area K_{ps} values in:		**p-value**
Spatial Region	**Time Period**	
Caudal	Acute	$p<0.0001$
Caudal	Subacute	$p<0.01$
Caudal	Chronic	$p<0.0001$
Epicenter	Acute	$p<10^{-5}$
Epicenter	Subacute	$p<10^{-7}$
Epicenter	Chronic	$p<10^{-6}$
Rostral	Acute	$p<0.03$
Rostral	Subacute	$p<0.001$
Rostral	Chronic	$p<0.0001$

Table 3

Summary of statistically significant association between K_{ps} and BBB scores

Association being tested	**Non-enhancing (NE) tissue**
Overall association between K_{ps} and BBB score	$p<0.001$
Association between K_{ps} and BBB score, by spatial region	Caudal region: $p<0.001$ Epicenter region: $p<0.001$ Rostral region: $p<0.001$
Interaction between region and BBB score, for K_{ps}	Epicenter region: $p<0.001$